TO APPEAR IN APJ LETTERS, OCTOBER 2001
Preprint typeset using LaTeX style emulateapj v. 14/09/00

arXiv:astro-ph/0109493v1 26 Sep 2001

EVIDENCE FOR JET DOMINATION OF THE NUCLEAR RADIO EMISSION IN LOW-LUMINOSITY ACTIVE GALACTIC NUCLEI

NEIL M. NAGAR[1], ANDREW S. WILSON[2], HEINO FALCKE[3]
To appear in ApJ Letters, October 2001

ABSTRACT

We present simultaneous, sub-arcsecond (≤ 50 pc) resolution 5 GHz, 8.4 GHz, and 15 GHz VLA[a] observations of a well-defined sample of sixteen low-luminosity active galactic nuclei (LLAGNs). The radio emission in most of these nuclei does not show the rising spectrum ($0.2 \lesssim s \lesssim 1.3$, $L_\nu \propto \nu^s$) expected from thermal electrons in an advection dominated accretion flow (ADAF) with or without weak to moderately-strong outflows. Rather, the flat radio spectra are indicative of either synchrotron self-absorbed emission from jets, convection-dominated accretion flows (CDAFs) with $L \gtrsim 10^{-5} L_{\rm Edd}$, or ADAFs with strong ($p \gtrsim 0.6$) outflows. The jet interpretation is favored by three factors: a) the detection of pc-scale radio extensions, morphologically reminiscent of jets, in the five nuclei with the highest peak radio flux-density; b) the domination of parsec-scale jet radio emission over unresolved 'core' emission in the three best-studied nuclei; and c) the lack of any clear correlation between radio spectral shape and black hole mass as would be expected from the dependence of the radio turnover frequency on black hole mass in ADAF and CDAF models. A jet domination of nuclear radio emission implies significantly lower accretion rates in ADAF-type models than earlier estimated from core radio luminosities.

[a] The VLA is operated by the National Radio Astronomy Observatory, a facility of the National Science Foundation operated under cooperative agreement by Associated Universities, Inc.

Subject headings: accretion, accretion disks — galaxies: active — galaxies: jets — galaxies: nuclei — radio continuum: galaxies — surveys

1. INTRODUCTION

The detection of optical broad-emission-lines (Ho et al. 1997b) and high brightness-temperature ($\gtrsim 10^8$ K) radio cores (Bietenholz et al. 2000; Junor & Biretta 1995; Falcke et al. 2000; Nagar et al. 2001) in the nuclei of a well-defined sample of nearby bright galaxies (Ho, Filippenko, & Sargent 1997a) indicates that at least 20% of all nearby bright galaxies have an accreting massive black hole. These nearby nuclei have been christened low-luminosity active galactic nuclei or LLAGNs. Their low nuclear luminosities require either very low accretion rates ($\sim 10^{-8} L_{\rm Edd}$; e.g. Falcke & Biermann 1999) or radiative efficiencies (the ratio of radiated energy to accreted mass) much lower than the typical value of $\sim$10% (e.g. Chapter 7.8 of Frank, King, & Raine 1995) assumed for powerful AGNs. This has led to renewed interest in spherical accretion models which produce low radiated luminosities, e.g. advection-dominated accretion flows (ADAFs; Narayan, Mahadevan, & Quataert 1998b), which may have associated outflows (Blandford & Begelman 1999), and convection-dominated accretion flows (CDAFs; Stone, Pringle, & Begelman 1999; Narayan et al. 2000; Quataert & Gruzinov 2000).

The sub-parcsec radio emission in LLAGNs may originate in an ADAF or CDAF inflow, and the predictions of these models are discussed in the following section. The sub-parsec radio emission may alternatively originate in synchrotron radiation from discrete plasma components or from the base of a continuous jet ejected from the central engine. In the former case, the presence of different self-absorption frequencies for individual components results in a flat spectral-shape ($s \sim 0$; $L_\nu \propto \nu^s$) for the overall system (e.g. Marscher 1988). In the latter case, i.e. for relativistic electrons at the base of a continuous, freely expanding jet (Blandford & Königl 1979), the variation of the electron density ($n_e \propto d^{-2}$), electron temperature ($T_{\rm ej} \propto d^0$), and magnetic field ($B \propto d^{-1}$), where d is the distance along the jet axis, results in a flat overall radio spectrum. Slightly inverted spectra (up to $s \simeq 0.2$) may result from the bulk acceleration of the jet plasma (Falcke 1996), and even higher (temporary) values of s may be measured during radio outbursts (e.g. Ho et al. 1999). On larger scales the synchrotron emission from the ejecta or jet becomes optically-thin ($s \simeq -0.7$). Thus the spectral index of the overall synchrotron emission from a 'jet' is expected to be between 0.2 and –0.7, depending on the relative contributions of the base and extended components.

2. RADIO SPECTRAL PREDICTIONS OF ADAFS AND CDAFS

In their simplest form ADAF and CDAF self-similar spherical models invoke standard α viscosity, a two-temperature thermal plasma, and a fixed ratio (β) of magnetic to gas pressure. Let us first use the analytic scaling-law approximations of Mahadevan (1997, hereafter M97) to estimate the expected radio spectral index in a self-similar flow. If we follow the derivation in Sec. 4.1 of M97 using magnetic field $B \propto r^{-c}$, electron temperature $T_e \propto r^{-a}$, and synchrotron emission factor $x_M \propto r^{-d}$ then the radio emission is self-absorbed, with spectral index $s \simeq \frac{5a+2c+2d-2}{2a+c+d}$ at frequencies below a critical frequency ν_p. Here r is the radius in units of the Schwarzschild radius and c is 5/4 in an ADAF (Narayan & Yi 1995) and 3/4 in a CDAF (Narayan et al. 2000). When $L \simeq 10^{-4} L_{\rm Edd}$, the dominance of synchrotron cooling forces a to 0 over the radio emitting region ($\lesssim 10^3$ r) in an ADAF or CDAF (see Narayan & Yi 1995).

[1] Arcetri Observatory, Largo E. Fermi 5, Florence 50125, Italy; neil@arcetri.astro.it
[2] Department of Astronomy, University of Maryland, College Park, MD 20742; wilson@astro.umd.edu; Adjunct Astronomer, Space Telescope Science Institute
[3] Max-Planck-Institut für Radioastronomie, Auf dem Hügel 69, 53121 Bonn, Germany; hfalcke@mpifr-bonn.mpg.de

However, when $L \lesssim 10^{-7} L_{\rm Edd}$ the electrons are adiabatically compressed so that $a \simeq 0.5$ in an ADAF (Narayan et al. 1998a) and $a \simeq 1$ (i.e. virial) in a CDAF (Narayan et al. 2000). The value of d is more difficult to estimate. M97 find $d \simeq 1/15$ in ADAFs with $L \simeq 10^{-4} L_{\rm Edd}$ (their Appendix B). Solving equation B1 of M97 with typical values of $T_e(r=1) = 10^9 - 10^{10}$ K and $m\dot{m} = 10^{-1} - 10^4$ shows that for an ADAF $d \simeq -0.15$ when $a = 0$ and $d \simeq -0.6$ when $a = 0.5$. Here m is the black hole mass in solar masses and $\dot{m}$ is the accretion rate in units of the Eddington rate (assuming 10% radiative efficiency). If we simplistically modify the form of ρ and B in an ADAF (equations 5 of M97) only in the power law dependence of r to convert them to the equivalent expresssions for a CDAF (see Narayan et al. 2000 for some justification of this), then we can solve the equivalent of M97's equation B1 to find that for a CDAF $d \simeq -0.2$ when $a = 0$ and $d \simeq -1.6$ when $a = 1$. Thus, for an ADAF one expects $0.2 \lesssim s \lesssim 1.1$ and for a CDAF one may expect $s = -1.8$ when $L \simeq 10^{-4} L_{\rm Edd}$ and $s = 1.1$ when $L \lesssim 10^{-7} L_{\rm Edd}$. Given the many approximations in this analytical method the above results should be considered only roughly indicative. ADAFs with outflows[4] have density profile $\rho \propto r^{-\frac{3}{2}+p}$ (Blandford & Begelman 1999) with p varying from 0 (no outflow) to 1 (strong outflow). The radio emission from the accretion flow corresponds to the ADAF case for $p = 0$ and to the CDAF case for $p = 1$; radio emission from the outflow has not been modeled and is not considered in this paper.

More accurate numerical modelling of the radio emission from an ADAF gives $s = 0.4$ when $L \simeq 10^{-4} L_{\rm Edd}$ (M97) and $s \simeq 1$ when $L \lesssim 10^{-7} L_{\rm Edd}$ with s decreasing but still positive as p increases from 0 to 0.6 (Narayan et al. 1998a; Quataert & Narayan 1999). To our knowledge, there has been no published work dealing explicitly with numerical modelling of the radio emission from a CDAF. In summary, the radio emission below ν_p from the accretion inflow of an ADAF or CDAF is expected to have a moderately to highly inverted spectrum except for a) CDAFs in systems with $L \gtrsim 10^{-5} L_{\rm Edd}$ and b) ADAFs with strong ($p \gtrsim 0.6$) outflows.

The inflow is optically thin at frequencies greater than

$$\nu_p = 1.3 \times 10^{-4} \alpha^{-1/2} (1-\beta)^{1/2} x_M m^{-1/2} \dot{m}^{1/2} T_e^2 \, r_{\rm min}^{-5/4} \qquad (1)$$

so the radio emission falls off exponentially above ν_p (M97). For ADAFs without outflows T_e and x_M are relatively independent of m for $m = 10^7$–$10^9\,{\rm M}_\odot$ (Fig. 2 of M97). Thus, for typical values of α (0.3), β (0.5), and $\dot{m}$ (10^{-4}–10^{-6}), one has $\nu_p \simeq 10^{15-16} m^{-1/2}$, i.e. the turnover frequency is greater than 15 GHz for all black holes considered here. In ADAFs with outflows and in CDAFs the flatter density profile results in a decrease in the values of T_e and B near $r \simeq 1$, and consequently a decrease in ν_p (and L_{ν_p}); the introduction of a moderately strong ($p = 0.6$) outflow to an ADAF can lower the value of ν_p by almost two orders of magnitude (Quataert & Narayan 1999).

3. OBSERVATIONS AND DATA REDUCTION

Sixteen of the 96 nearest (D $\leq$ 19 Mpc) LLAGNs from the Palomar sample (Ho et al. 1997a) have a highly compact ($\lesssim$ 2 mas), high brightness-temperature ($\gtrsim 10^8$ K) radio core (see Falcke et al. 2000; Nagar et al. 2001). These sixteen LLAGNs, listed in Table 1, were observed with the Very Large Array (VLA) at 5 GHz (6 cm), 8.4 GHz (3.6 cm), and 15 GHz (2 cm). The observations were made on September 5 and September 10, 1999, while the VLA was in "A"-configuration (see Thompson et al. 1980). Each LLAGN observation was sandwiched between two observations of a nearby phase-calibrator with typical cycle times, in minutes, of 1-7-1, 1-6-1, and 2-7-2, at 5 GHz, 8.4 GHz, and 15 GHz, respectively. The observations at the three frequencies are simultaneous to $\leq$30 min for each LLAGN.

Data were calibrated and mapped using the AIPS software, following the standard procedures outlined in the AIPS cookbook. Observations of 3C 147 and 3C 286 were used to set the 5 GHz flux-density scale, and observations of 3C 286 were used to set the 8.4 GHz and 15 GHz flux-density scales. The 15 GHz observation of 3C 286 was made at a single (1.4) airmass, and all 15 GHz observations were made at airmasses of 1.06 to 1.4, so the 15 GHz flux calibration error from elevation effects is expected to be less than 0.2% (Perley 2000). For this reason we did not make elevation-dependent gain corrections to the 15 GHz data. The VLA documentation suggests that the flux calibration at 5 GHz and 8.4 GHz should be accurate to 1%–2%, and that at 15 GHz should be accurate to 3%–5%; we conservatively use the higher numbers as the respective $2\,\sigma$ errors. For sources with flux greater than 3 mJy, we were able to iteratively self-calibrate (both phase-only and amplitude-and-phase) and image the data so as to increase the signal-to-noise ratio in the final map. The root mean square noise in the final uniformly weighted maps was typically 100 μJy, 60 μJy, and 170 μJy at 5 GHz, 8.4 GHz, and 15 GHz, respectively. The resolution at these three wavelengths was typically 0.″5, 0.″27 and 0.″15, respectively. We also made 15 GHz and 8.4 GHz maps with the same resolution (0.″5) as the 5 GHz maps, by appropriately tapering the (u,v) data.

4. RESULTS

All sources except NGC 4168 at 15 GHz were clearly detected in initial (non-self-calibrated) maps. The 15 GHz observation of NGC 4168 was made during very bad weather, and we were able to make a noisy map only after self-calibration with a point-source model. The newly measured flux-densities are listed in Table 1. The 15 GHz data are noisy because of bad weather and high humidity. Therefore the three nuclei for which we could not self-calibrate the 15 GHz data have true 15 GHz fluxes somewhere between the measured values and 3 mJy. For all but three of the objects, the radio emission at all three frequencies is compact; a Gaussian fit to the source does not give a deconvolved size more than half a beam-size. The three sources with detected extended structure are all previously known to have such structure: NGC 4278 (Wilkinson et al. 1998), NGC 4472 (Ekers & Kotanyi 1978), and NGC 4486 (M 87; e.g. Junor & Biretta 1995). The unresolved emission dominates the extended emission in our maps of these three sources except in NGC 4472, which has a very weak core. Most nuclei have roughly similar fluxes in the full resolution 15 GHz maps and the 0.″5 resolution tapered maps (Table 1); the same is true at 8.4 GHz. The peak flux-density in the 0.″5 resolution, 5 GHz VLA maps is $\sim$0.8–2.1 times the total (but not necessarily core) flux in the central $\leq$20 mas of the 5 GHz (non-simultaneous) VLBA maps for all sources which were observed in our June 1997 and April 1999 VLBA runs (column 14 of Table 1).

The variation of the core spectral index (from the peak fluxes in matched resolution maps) with black hole mass is shown in Fig. 1a. We have distinguished between black hole masses

[4] CDAFs are considered separate from "outflows" as their convective eddies are not unbound (Narayan et al. 2000).

derived directly from stellar-, gas-, and maser-dynamics (Gebhardt et al. 2000; Richstone et al. 1998) from those inferred from central velocity dispersions (using the relationship derived by Gebhardt et al. 2000) and galaxy bulge masses (using the relationship derived by Richstone et al. 1998). Only NGC 3031 (M 81) and NGC 4772 consistently show the highly inverted radio spectrum expected in ADAF models with or without weak to moderately-strong outflows. The core radio emission from the latter galaxy is probably dominated by extended emission (see above), and as discussed below the radio emission from the former is probably from a jet. Apart from NGC 4472, the elliptical galaxies have a similar spectral shape above and below 8.4 GHz. Most of the non-ellipticals have a spectrum which falls more rapidly at frequencies above 8.4 GHz than below (Fig. 1b), with NGC 3718 and NGC 4258 being the exceptions. When high ($\leq 2''$) resolution 2-10 keV X-ray luminosities are available (e.g. Ho et al. 2001), the ratio of νL_ν between X-ray and radio is $\sim 10^{1-3}$, suggestive of strong outflows in an ADAF scenario (Di Matteo, Carilli, & Fabian 2001). Interestingly, this ratio is $\gtrsim$100 for the Seyfert 1s and $\lesssim$100 for the other nuclei.

5. DISCUSSION

Very low accretion rates (perhaps due to convection or strong outflows) may cause ν_p to fall close to 5–15 GHz for the objects in the sample. Such a scenario is supported by the evidence for turnover frequencies in the 10–30 GHz range for a few ellipticals (Di Matteo et al. 2001). If this is the case, then eqn. 1 implies lower values of ν_p for more massive black holes. That is, within our sample we would expect nuclei with less massive black holes to have more inverted spectra than nuclei with more massive black holes. However, even though we sample more than two orders of magnitude in m, Fig. 1 does not support such a trend. Therefore, unless non-ellipticals have different micro-physical parameters, or higher accretion rates, or a different accretion mechanism, as compared to ellipticals, it is unlikely that a turnover frequency in the 5–15 GHz range is the cause of the observed flat radio spectrum in most of the sample. If $\nu_p > 15$ GHz for most nuclei in the sample, then any inverted spectrum radio component must be dominated by other sources at 5 GHz and 8.4 GHz (and perhaps even at 15 GHz). One potential source is non-thermal electrons within the ADAF (Özel, Psaltis, & Narayan 2000). Significant emission from star-formation related processes can be ruled out as the radio core has a high brightness-temperature at 5 GHz, and at this wavelength most of the flux within the central $0.''5$ is also detected on mas-scales (Table 1). On the other hand, the observed distribution of spectral indices is consistent with the 5–15 GHz radio emission originating in synchrotron-emitting jets.

Whether or not an accretion flow contributes to the nuclear radio emission, the detections of what appear to be collimated pc-scale jets in the five LLAGNs of Table 1 with the highest core flux - NGC 3031 (M 81; Bietenholz et al. 2000), NGC 4278 (Jones, Wrobel, & Shaffer 1984; Falcke et al. 2000), NGC 4486 (M 87; Junor & Biretta 1995), NGC 4374 (M 84; Wrobel, Walker, & Bridle 1996; Nagar et al. 2001), and NGC 4552 (M 89; Nagar et al. 2001) - does indicate that synchrotron emission from jets is a significant contributor to the sub-arcsecond radio emission. In fact, in all three sample nuclei which have been comprehensively studied at high resolution in the radio, the radio flux from the jet dominates that from the unresolved "core." In NGC 4486 the jet component within 30 mas (2.5 pc) of the nucleus contributes three times the radio flux of the unresolved (1 mas x 0.2 mas) "core" (Junor & Biretta 1995). Given that this "core" continues to be further resolved at higher resolutions (Junor, Biretta, & Livio 1999), and that the jet is a strong radio emitter on scales of 30 mas to $1''$, the jet is certainly the dominant sub-arcsecond radio emitter. In NGC 3031, which has a spectral shape consistent with an ADAF model, sub-mas multi-epoch observations reveal that the sub-parsec jet contributes at least three times the radio flux of the unresolved "core" (Bietenholz et al. 2000). Deep radio observations of NGC 4258 not only reveal a sub-parsec jet, but also indicate an absence of continuum emission from the putative location (as traced by the water-vapour maser disk) of the nucleus (Herrnstein et al. 1997).

In the context of any low-luminosity spherical accretion model, the presence of outflows and the smaller radio luminosities attributable to the inflow both point to accretion rates at least an order of magnitude lower than than earlier predicted using ADAF models (e.g. 10^{-2}–$10^{-4}\ L_{\rm Edd}$; Chang, Choi, & Yi 2000; Yi & Boughn 1999). A jet can also cause considerable disruption of the high-frequency radio emitting region ($\sim 1r - 100r$) of the inflow. Junor et al. (1999) find a wide ($\gtrsim 60^\circ$) initial opening angle for the (potentially relativistic) radio jet in NGC 4486, with collimation only occurring at $\sim 100r$. For a moderately-strong outflow (e.g. $p = 0.6$) about 25% of the material accreted at $100r$ is lost to the outflow by $2r$. Thus it may not be accurate to model the radio emitting region as a spherical self-similar flow in which the only effect of the outflow is a modification of the accretion rate and central density.

REFERENCES

Bietenholz, M. F., Bartel, N., & Rupen, M. P., 2000, ApJ, 532, 895
Blandford, R. D., & Begelman, M. C. 1999, MNRAS, 303, L1
Blandford, R. D., & Königl, A. 1979, ApJ, 232, 34
Chang, H., Choi, C., & Yi, I., ApJ, submitted (astro/ph-0009267)
Di Matteo, T., Carilli, C. L., & Fabian, A. C. 2001, 2001, ApJ, 547, 731
Ekers, R. D., & Kotanyi, C. G. 1978, A&A, 67, 47
Falcke, H. 1996, ApJ, 464, L67
Falcke, H. & Biermann, P. L. 1999, A&A, 342, 49
Falcke, H., Nagar, N. M., Wilson, A. S., & Ulvestad, J. S. 2000, ApJ, 542, 197
Frank, J., King, A., & Raine, D. 1995, in Accretion Power in Astrophysics, 2nd edition, (Cambridge: Cambridge Univ. Press)
Gebhardt, K., et al. 2000, ApJ, 539, L13
Herrnstein, J. R., Moran, J. M., Greenhill, L. J., Diamond, P. J., Miyoshi, M., Nakai, N., & Inoue, M. 1997, ApJ, 475, L17
Ho, L. C., et al. 2001, ApJ, 549, L51
Ho, L. C., Filippenko, A. V., & Sargent, W. L. W. 1997a, ApJS, 112, 315
Ho, L. C., Filippenko, A. V., & Sargent, W. L. W., & Peng, C. Y. 1997b, ApJS, 112, 391
Ho, L. C., van Dyk, S. D., Pooley, G. G., Sramek, R. A., & Weiler, K. W. 1999, ApJ, 118, 843
Jones, D. L., Wrobel, J. M., & Shaffer, D. B. 1984, ApJ, 276, 480
Junor, W., & Biretta, J. A. 1995, AJ, 109, 500
Junor, W., Biretta, J. A., & Livio, M. 1999, Nature, 401, 891
Mahadevan, R. 1997, ApJ, 477, 585 (M97)
Marscher, A. P. 1988, ApJ, 334 552
Nagar, N. M., Wilson, A. S., Falcke, H., & Ulvestad, J. S. 2001, in preparation
Narayan, R., Igumenshchev, I. V., & Abramowicz, M. A. 2000, ApJ, 539, 798
Narayan, R., Mahadevan, R., Grindlay, J. E., Popham, R. G., & Gammie, C. 1998a, ApJ, 492, 554
Narayan, R., Mahadevan, R., & Quataert, E. 1998b, in The Theory of Black Hole Accretion Discs, ed. M. A. Abramowicz, G. Björnsson, & J. E. Pringle (Cambridge: Cambridge Univ. Press), 148
Narayan, R., & Yi, I. 1995, ApJ, 452, 710
Özel, F., Psaltis, D., & Narayan, R. 2000, ApJ, 541, 234
Perley, R. A. 2000, in VLA Observational Status Summary, available on-line at www.nrao.edu

Quataert, E., & Gruzinov, A. 2000, ApJ, 539, 809
Quataert, E., & Narayan, R. 1999, ApJ, 520, 298
Richstone, D., et al. 1998, Nature, 395A, 14
Stone, J. M., Pringle, J. E., & Begelman, M., C. 1999, MNRAS, 310, 1002
Thompson, A. R., Clark, B. G., Wade C. M., & Napier, P. J. 1980, ApJS, 44, 151
Wilkinson, P. N., Browne, I. W. A., Patnaik, A. R., Wrobel, J. M., & Sorathia, B. 1998, MNRAS, 300, 790
Wrobel, J. M., Walker, R. C., & Bridle, A. H. 1996, in Extragalactic radio sources: proc. of the 175th Symposium of the IAU, ed. R. D. Ekers, C. Fanti, & L. Padrielli (Kluwer Academic Publishers), 131
Yi, I., & Boughn, S. P. 1999, ApJ, 515, 576

Table 1. MULTI-FREQUENCY OBSERVATIONS OF LLAGNs WITH THE VLA

Galaxy	Act.	T	5 GHz flux (mJy)		8.4 GHz flux (mJy)				15 GHz flux (mJy)				VLA/
Name	Type		full resolution		full resolution		0.″5 resolution		full resolution		0.″5 resolution		VLBA
			Peak	Total	Peak	Total	Peak	Total	Peak	Total	Peak	Total	
(1)	(2)	(3)	(4)	(5)	(6)	(7)	(8)	(9)	(10)	(11)	(12)	(13)	(14)
NGC 2787	L1.9	−1	15.7	15.8	15.6	15.6	15.6	15.6	13.0	13.5	13.6	13.7	1.4
NGC 3031	S1.5	2	208.7	209.1	278.6	278.7	278.7	279.1	338.3	340.6	340.9	341.5	···
NGC 3718	L1.9	1	6.8	7.0	6.6	6.6	6.7	6.6	11.5	12.1	11.2	12.3	1.3
NGC 4143	L1.9	−2	8.3	8.5	7.8	7.9	7.9	7.9	4.5	4.9	5.4	5.5	1.0
NGC 4168	S1.9	−5	4.7	4.8	3.9	3.8	3.8	3.6	2.9	3.0	3.3	3.5	2.0
NGC 4203	L1.9	−3	10.8	11.2	10.6	10.7	10.6	10.7	11.2	11.2	10.8	12.1	1.2
NGC 4258	S1.9	4	1.6	2.1	1.5	1.8	1.6	1.9	2.3	2.5	2.2	2.8	···
NGC 4278	L1.9	−5	143.9	159.8	105.9	113.5	111.8	120.7	77.2	79.9	80.1	81.3	1.6
NGC 4374	L2	−5	168.7	167.6	163.1	165.2	165.0	166.5	165.3	168.0	167.3	168.2	0.9
NGC 4472	S2	−5	4.8	4.8	4.7	4.7	7.2	7.2	2.5	2.5	4.3	4.3	2.1
NGC 4486	L2	−4	2875.1	3097.1	2368.6	2573.3	2537.9	2638.9	1976.5	2289.9	2175.6	2295.5	···
NGC 4552	T2	−5	131.1	131.7	104.0	105.0	104.8	105.2	82.0	83.7	83.7	84.9	0.9
NGC 4565	S1.9	3	2.5	2.5	2.4	2.4	2.4	2.5	1.8	1.9	1.5	3.1	0.8
NGC 4579	S1.9	3	26.1	29.1	25.6	27.5	27.1	27.9	22.0	23.6	23.5	24.1	1.2
NGC 4772	L1.9	1	1.8	1.9	2.9	2.9	2.8	2.8	3.3	3.9	3.6	5.1	1.4
NGC 5866	T2	−1	12.4	12.7	11.2	11.5	11.4	11.7	9.2	9.3	8.5	8.9	1.5

Note. — Columns are: (1) galaxy name; (2) nuclear activity type as derived by Ho et al. (1997a). 'L' represents LINER, 'S' represents Seyfert, 'H' represents an H II region type spectrum, and 'T' represents objects with transitional 'L' + 'H' spectra. '2' implies that no broad Hα is detected, '1.9' implies that broad Hα is present, but not broad Hβ, and '1.5' implies that broad Hα and broad Hβ are detected; (3) the morphological type of the host galaxy as listed in Ho et al. (1997a); (4) and (5) peak flux-density and total flux (mJy) of the core at 5 GHz in the highest ($\sim 0.''5$) resolution VLA maps; (6) and (7) peak flux-density and total flux (mJy) of the core at 8.4 GHz in the highest ($\sim 0.''3$) resolution VLA maps; (8) and (9) peak flux-density and total flux (mJy) of the core at 8.4 GHz, in maps tapered to $0.''5$ resolution; (10) and (11) peak flux-density and total flux (mJy) of the core at 15 GHz in the highest ($\sim 0.''15$) resolution VLA maps; (12) and (13) peak flux-density and total flux (mJy) of the core at 15 GHz, in maps tapered to $0.''5$ resolution; (14) ratio of the peak 5 GHz VLA flux ($0.''5$ resolution) to the total 5 GHz flux in the inner $\sim$20 mas of (non-simultaneous) VLBA maps, for nuclei observed with the VLBA by Falcke et al. (2000) and Nagar et al. (2001).

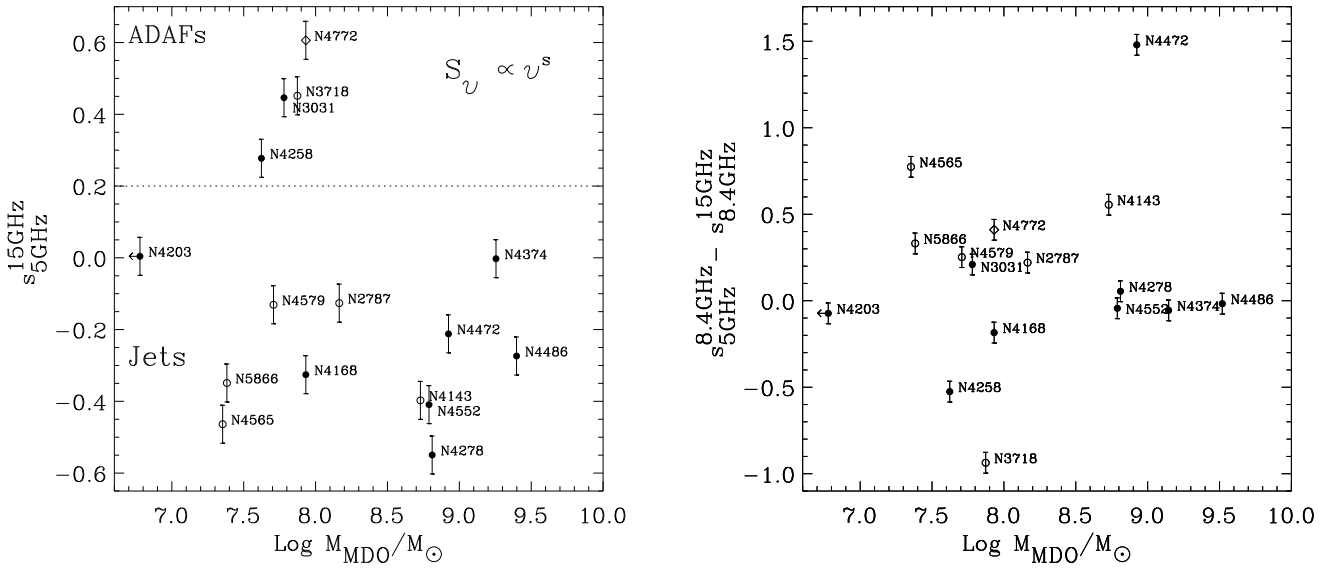

FIG. 1.— The (a) spectral index and (b) change in the spectral index, between 5 GHz and 15 GHz, as a function of black hole mass. Nuclei with positive *y*-axis values in (b) have spectra which fall off more steeply above 8.4 GHz than below. Filled black circles are used for reliable black hole estimates, and open circles and open diamonds are used for black hole masses inferred from the relationships of Gebhardt et al. (2000) and Richstone et al. (1998), respectively (see text). Two sigma error bars in *y* are shown.